

Hoechst Is All You Need: Lymphocyte Classification with Deep Learning

Jessica Cooper*, In Hwa Um,
Ognjen Arandjelović and David J Harrison

*jmc31@st-andrews.ac.uk
University of St Andrews
July 19, 2021

1 Abstract

Multiplex immunofluorescence and immunohistochemistry benefit patients by allowing cancer pathologists to identify several proteins expressed on the surface of cells, enabling cell classification, better understanding of the tumour micro-environment, more accurate diagnoses, prognoses, and tailored immunotherapy based on the immune status of individual patients. However, they are expensive and time consuming processes which require complex staining and imaging techniques by expert technicians. Hoechst staining is much cheaper and easier to perform, but is not typically used in this case as it binds to DNA rather than to the proteins targeted by immunofluorescent techniques, and it was not previously thought possible to differentiate cells expressing these proteins based only on DNA morphology. In this work we show otherwise, training a deep convolutional neural network to identify cells expressing three proteins (T lymphocyte markers CD3 and CD8, and the B lymphocyte marker CD20) with greater than 90% precision and recall, from Hoechst 33342 stained tissue only. Our model learns previously unknown morphological features associated with expression of these proteins which can be used to accurately differentiate lymphocyte subtypes for use in key prognostic metrics such as assessment of immune cell infiltration, and thereby predict and improve patient outcomes without the need for costly multiplex immunofluorescence.

2 Introduction

Among patients with cancers of the same stage, clinical outcomes vary widely. This is thought to be in large part due to the complex interaction between tumour cells and the immune response of individual patients, as the proportion, location, and sub-type of lymphocytes present in the tissue has been shown to

have important implications for patient prognosis [4, 19]. There exist proprietary methods to assess immune cell infiltration, which formally quantify CD3+ and CD8+ T cell lymphocytes both in the centre of tumour and in the invasive margin, as proposed by Galon et al. [9]. Combining their evaluation with T-and-B score (CD8+ T cell and CD20+ B cell) as per Mlecnik et al. had significant predictive power for colorectal cancer patient survival [33, 19], and compared to to the latest guidelines of the American Joint Committee on Cancer/ Union for International Cancer Control (AJCC/ UICC) tumour-node-metastasis (TNM) classification, immune cell infiltration evaluation alone has shown superior prognostic value in international studies of stage I-IV colon cancer patients, and has life-saving applications in clinical decision-making [30, 31, 24, 23, 4, 9, 10]. However, in order to identify the CD3, CD8 and CD20 expressing cells necessary to calculate these valuable metrics, either multiple immunohistochemistry or multiplexed immunofluorescence are required – both of which are time consuming and expensive protocols [33, 2]. Using contemporary equipment, three simultaneous rounds of immunohistochemistry takes around three hours and costs approximately \$20 in reagents, whilst multiplex immunofluorescence requires 9 hours and the associated reagents cost upward of \$70 for a single slide. In this work we show that costly protocols of this type are in fact unnecessary – it is possible to accurately identify CD3, CD8 and CD20 expressing lymphocytes from common and inexpensive stains. Hoechst and DAPI (popular blue fluorescent, nuclear-specific dyes [22, 6, 7]) are far cheaper and easier to perform, costing pennies and requiring just ten minutes per slide. DAPI has better photostability, but since our slides could be imaged immediately in this work we use Hoechst 33342 due to its superior signal-to-noise (genuine DNA stain/autofluorescence) ratio.

2.1 Artificial Intelligence and Digital Pathology

Deep learning techniques are increasingly used in digital pathology to assist human experts with a range of diagnostic and prognostic tasks. The data used to train these models often takes the form of whole slide images (WSIs) with associated labels. One application of deep learning in this field is *segmentation* – that is, given some input image, learning to produce class labels for each pixel in that image. For example, given a set of biopsy slides which have been divided into cancerous and non-cancerous regions by a human annotator, we could train a neural network model to label each pixel in the image as cancerous or non-cancerous [32, 14, 15, 5]. This is distinct from *classification* tasks, in which a single label is provided for an entire slide or region, and pixel-level classification is not required.

For image segmentation tasks Convolutional Neural Networks (CNNs) are most widely used [29]. One type of CNN is the U-Net [26] – a type of residual neural network [11] – so named for its 'U' shaped architecture. Residual neural networks in general, and the U-Net in particular, are well suited for segmentation tasks as they allow spatial information from the input to propagate directly to the output. Recent work using U-Nets has shown great promise for digital

pathology applications [21, 20, 13, 18, 1, 12], but publications to date have focused on automating tasks that human experts can already do. In this work we take a different approach, asking instead – can a deep neural network learn to do something that human experts cannot?

3 Materials and Methods

Our data comprised six Whole Slide Images (WSIs) taken from lung cancer biopsies. These were imaged using Hoechst 33342, and also using multiplex immunofluorescence targeting CD3, CD8 and CD20 expressing immune cells, with a Zeiss Zen Axioscan scanner. We then used an established intensity-based classification technique [25] to identify and label cells expressing these proteins in the multiplex immunofluorescence images, the results of which we quality controlled by direct visual inspection to ensure label accuracy. To handle varying levels of co-expression within CD3 and CD8 expressing cells we used a labelling threshold to classify each cell into one of five groups based on protein expression: CD3 only; CD8 and low CD3 (labelled CD8_CD3LO); CD8 and high CD3 (labelled CD8_CD3HI); CD20 only; and background/other. We used these labels to create segmentation maps, which we paired with the Hoechst images, as in Figure 1.

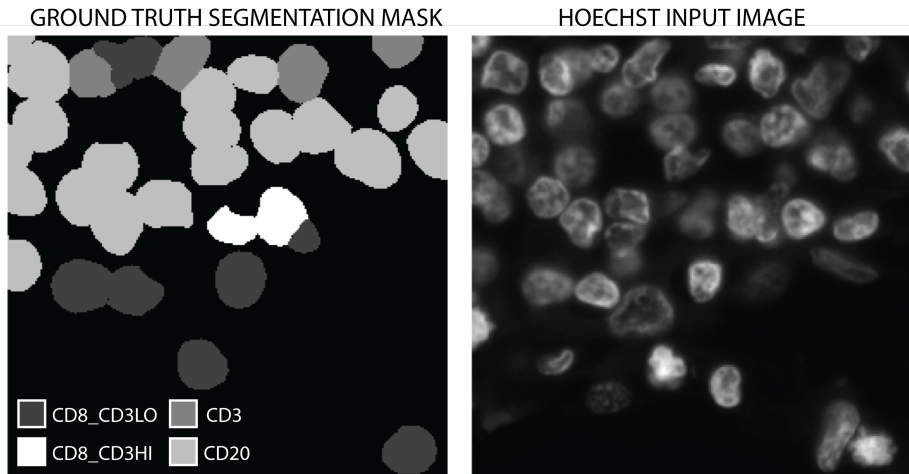


Figure 1: Labelled immune cell mask from multiplex immunofluorescence image (left) and corresponding Hoechst 33342 stained patch (right).

We used these image pairs to train a semantic segmentation model with U-Net architecture [26] and a resnet34 encoder [11] to output a segmentation map for each class, taking only a Hoechst image as input.

3.1 Data Source

The slides we used were provided by NHS Lothian via David J Harrison. Our six slides were selected for their greater frequency of immune cells from a larger cohort of consenting early-stage lung adenocarcinoma patients.

3.2 Multiplexed Immunofluorescence (mIF) Protocol

Leica BOND RX automated immunostainer (Leica Microsystems, Milton Keynes, UK) was utilised to perform mIF. The sections were dewaxed at 72°C using BOND dewax solution (Leica, AR9222) and rehydrated in absolute alcohol and deionised water, respectively. The sections were treated with BOND epitope retrieval 1 (ER1) buffer (Leica, AR9961) for 20 min at 100°C to unmask the epitopes. The endogenous peroxidase was blocked with peroxide block (Leica, DS9800), followed by serum free protein block (Agilent, x090930-2). The sections were incubated with the first primary antibody (CD20, Agilent, M075501-2, 1:400 dilution) for 40 min at room temperature, followed by anti-mouse HRP conjugated secondary antibody (Agilent, K400111-2) for 40 min. Then CD20 antigen was visualised by fluorescein conjugated tyramide signal amplification (TSA) (Akoya Bioscience, NEL741001KT). Redundant antibodies, which were not covalently bound, were stripped off by ER1 buffer at 95°C for 20 min. Then the second primary antibody (CD8, Agilent, M710301-2, 1:400 dilution) was visualised by TSA Cy3, taking the same steps from peroxide block to the ER1 buffer stripping of the first antibody visualisation. Lastly, the sections were incubated with the last primary antibody (CD3, Agilent, A045229-2, 1:70 dilution), followed by biotinylated anti-rabbit secondary antibodies (Thermo fisher, 65-6140), which was visualised by Alexa flour 750 conjugated streptavidin (Thermo fisher, S21384). Cell nuclei were counterstained by Hoechst 33342 (Thermo fisher, H3570, 1:100) and the sections were mounted with prolong gold antifade mountant (Thermo fisher, P36930).

3.3 Image Acquisition and Analysis

Zeiss Axio scan z1 was utilised to capture fluorescent images. Four different fluorescent channels (Hoechst3334, Fluorescein, Cy3 and AF750) were simultaneously used to capture individual channel images under 20x object magnification. The exposure time of four channels (Hoechst33342, Fluorescein, cy3 and AF750) were 8 milliseconds, 20 ms, 50 ms, and 800 ms, respectively. The image was generated in czi format.

The fluorescent images were opened in QuPath v.0.2.3 [3]. StarDist [27] was utilised to segment cell nuclei using StarDist2D builder. The probability threshold of cell detection, pixel size and the cell expansion was 0.6, 0.2270 and 1.0, respectively. The object classifier was utilised to classify CD20, CD8 and CD3 cells by the intensity threshold of fluorescein, Cy3 and AF750 channels, which were 5000, 4000 and 2200, respectively.

We extracted 7413 256×256 pixel patches with a 50% overlap from the

	CD8_CD3LO	CD3	CD20	CD8_CD3HI	Other
Count	14536	14480	7528	1412	153811
Presence	5259	4955	1352	1071	7375
Coverage	7.6%	7.5%	3.9%	0.7%	80.2%

Table 1: Class representation across the dataset: the total number of cells present (Count); the number of samples containing at least one cell of that type (Presence); and the total pixel percentage of input covered each cell type (Coverage).

Hoechst 33342 stained slides at full resolution, and paired them with the per-pixel class labels from the immunofluorescence intensity classifier as shown in figure 1. Each Hoechst patch was normalised individually, and the total dataset split into training, validation and testing subsets with ratio 80:10:10, providing 5930 training samples, 741 validation samples, and 742 test samples. We also tested training the model on five of the six slides, retaining the sixth as a holdout test set in order to ascertain the generalisation ability, and found no decrease in performance.

This dataset exhibited some class imbalance, with most of the total input consisting of background or cells expressing none of the proteins that we are concerned with. CD8_CD3LO expressing lymphocytes formed the majority of positive examples, closely followed by CD3. CD20 and CD8_CD3HI were rarer, as shown in Table 1.

3.4 Model Architecture and Training

All computation was performed using NVIDIA GeForce RTX 2060. We trained the model over 100 epochs using a batch size of 32, an initial learning rate of 0.001, AdamW optimisation [17], and cross-entropy loss $-\sum_{c=1}^C \tau_c \log(\rho_c)$ on the $\text{Softmax}(x_i) = \frac{e^{x_i}}{\sum_{c=0}^C e^{x_c}}$ output. This protocol was designed after significant experimentation, considering a range of architectures and hyperparameters. We found that deeper encoders and other segmentation models provided in the Segmentation Models Pytorch library [34] provided either no significant increase proportional to computation cost, or a decrease in model performance. We also explored the use of focal loss [16] to address class imbalance, but found no improvement in performance.

4 Results

To evaluate model performance for each class we used a number of established metrics for semantic segmentation tasks of this type as shown, comprising precision P , recall R and F1 score F , where target $\tau \in \{0, 1\}$ is the $d \times d$ pixel-wise ground truth map for that class, and output $\rho \in [0, 1]$ the $d \times d$ softmaxed model prediction.

Per-Pixel	F1	Precision	Recall
CD8_CD3LO	0.96 / 0.92	0.96 / 0.95	0.96 / 0.90
CD3	0.96 / 0.91	0.96 / 0.90	0.96 / 0.92
CD20	0.97 / 0.93	0.96 / 0.96	0.97 / 0.90
CD8_CD3HI	0.95 / 0.89	0.95 / 0.88	0.95 / 0.91
Avg.	0.96 / 0.91	0.96 / 0.91	0.96 / 0.91
Per-Centroid	F1	Precision	Recall
CD8_CD3LO	0.99 / 0.96	0.99 / 0.98	0.99 / 0.94
CD3	0.99 / 0.96	0.99 / 0.95	0.99 / 0.96
CD20	1.00 / 0.97	1.00 / 0.99	1.00 / 0.95
CD8_CD3HI	0.99 / 0.92	0.99 / 0.91	0.99 / 0.95
Avg.	0.99 / 0.95	0.99 / 0.96	0.99 / 0.95

Table 2: Mean per-pixel and per-centroid segmentation performance on training set / holdout test set.

These metrics were also applied using only the centroid coordinates of each cell – due to the nature of the task at hand, identifying which proteins are present and their location is more relevant than perfectly segmenting each individual cell, and as such we do not wish to unduly penalise the model if it correctly locates and classifies a protein expressing cell, but fails to capture the exact shape of that cell.

$$\begin{aligned}
tp &= \sum_{x,y=0}^d \tau_{x,y} \rho_{x,y} \\
tn &= \sum_{x,y=0}^d (1 - \tau_{x,y})(1 - \rho_{x,y}) \\
fp &= \sum_{x,y=0}^d \rho_{x,y}(1 - \tau_{x,y}) \\
fn &= \sum_{x,y=0}^d \tau_{x,y}(1 - \rho_{x,y}) \\
P &= \frac{tp}{tp + fp} \quad R = \frac{tp}{tp + fn} \quad F1 = \frac{2PR}{P + R}
\end{aligned} \tag{1}$$

Table 2 shows the performance of our model according to these metrics. We achieve over 90% precision, recall and F1 score across all classes on the test set, showing excellent generalisation ability to unseen data with only a small decrease in performance compared to the training set. CD8_CD3HI expressing cells were the most difficult to classify, likely due to their lower representation across the training set. As expected, we see a small increase in performance across these metrics when evaluating the cell centroid classifications only, because in this case imperfect segmentation of regions at the edges of cells is disregarded. Figure 2

shows four random sample pairs from the test set, along with the model output predictions for each class – as we can see here, the segmentation is reliably good.

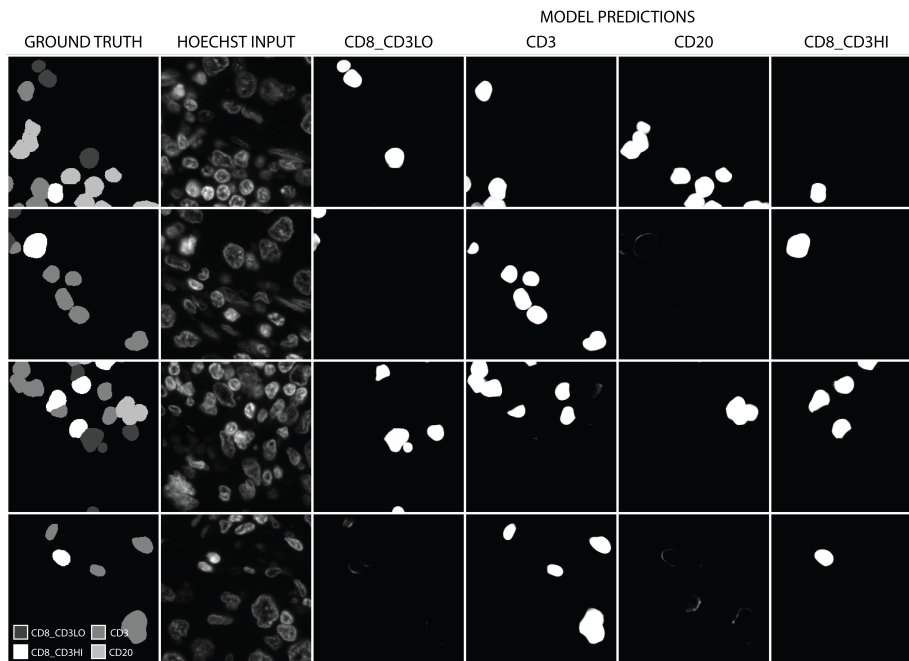


Figure 2: Examples of model predictions on test set images – here we show the ground truth segmentation mask of class labels, the Hoechst 33342 stained input image, and the predicted segmentation output for each class.

5 Discussion

To explore how the network is able to distinguish between different lymphocytes so successfully, we use stochastic gradient descent (SGD) to optimize an input image I set uniformly to the normalised mean of all training set images to maximise output logits (raw outputs, without activation or normalisation) for each class, as proposed by Simonyan et al. [28]. We extend this technique for multi-class segmentation using a custom loss function designed to balance per-class optimisation for class-specific quadrants in a single image, allowing for easy comparison of learned features.

5.1 Feature Visualisation

For input image optimisation we used a learning rate of 1.0 and ran SGD for 10,000 steps. We optimise each quadrant for a different positive class (i.e. those classes not consisting of background or cells outwith our classes of focus), by

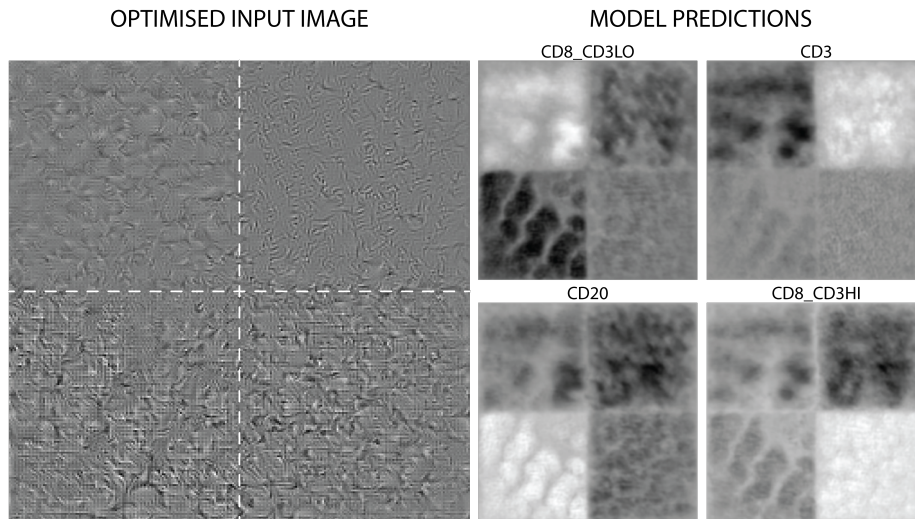


Figure 3: Optimised input image generated using stochastic gradient descent to maximise class predictions for each quadrant.

specifying a mask μ of dimension $C \times d \times d$ (where d is the x and y dimension of the input image – in this case 256 pixels – and C is the number of positive classes – in this case 4) such that for each class c in C a different quadrant is set to ones, and the remaining elements in c to zero – the objective being to maximise the model outputs for each class in a specific region, as shown in Figure 3. This mask is used to separate pixels to maximise and those to minimise in the model outputs ρ according to class. The Rectified Linear Unit (ReLU) is applied to the regions to minimise, to control for disproportionate minimisation of negative regions in preference to the positive regions, in which we are interested. We also use a regularisation term consisting of the variance between positive class outputs to ensure that the input is not disproportionately maximised for classes associated with simpler features, as shown below. Simonyan et al. included an additional L_2 regularisation term for the input image I to counteract over-optimisation for a single feature, but in practice we found that this lead to negligible change in output and so we omit it – likely this omission is possible because we are optimising for mean pixel classifications and thereby for multiple features, rather than for a single label.

$$\begin{aligned}
ReLU(x) &= \begin{cases} 0 & \text{if } x < 0 \\ x & \text{otherwise} \end{cases} \\
V(x) &= \frac{\sum_i (x_i - \bar{x})^2}{C} \\
Loss &= \frac{1}{d^2 C} \sum_{c=0}^C \sum_{x,y=0}^d ReLU(\rho_{c,x,y} |\mu_{c,x,y} - 1|) - \mu_{c,x,y} \rho_{c,x,y} \\
&\quad + V \left(\left[\frac{1}{d^2} \sum_{x,y=0}^d ReLU(\rho_{c,x,y} |\mu_{c,x,y} - 1|) - \mu_{c,x,y} \rho_{c,x,y} \text{ for } c = 1 \dots C \right] \right)
\end{aligned} \tag{2}$$

As shown in Figure 3, the results of this experiment show that the model has learned textural features of the nuclear chromatin to discriminate between different classes, as the predominant difference between regions is textural and evident features are small. This difference in texture is particularly pronounced between CD8_CD3LO and CD3 only expressing cells, with the CD3 only class quadrant in particular optimising for quite small, curved features. In models like ours where the output class probabilities for each pixel are calculated – and thereby constrained and exaggerated – through use of softmax as an output function, it is difficult to differentiate a strong positive signal for an individual class from a strong negative signal for the *other* classes. This also holds for the logits which we here hope to maximise for each class – in the context of actual predictions by the model, these logits would be passed into a softmax function, and as such interact in a way we so not visualise here – for example, classes A and B may have a high logit output, but if A is lower than B, the softmaxed output will strongly favour B even if the raw difference in output was not great. This makes optimisation-based visualisation of features in this way problematic: if we optimise for softmaxed outputs, the output is quickly saturated and the inputs are unintelligible, but if we optimise for logits, we do not accurately represent the actual classifications of the entire model.

To gain further insight into the learned features, we used Hierarchical Perturbation [8] (HiPe) to generate saliency maps – visualisations of which regions of the input image were more or less important in determining the ultimate output of the model – at different resolutions, as shown in Figure 4. We used the standard implementation of HiPe on the softmaxed output of the model, with “fade” perturbation (such that occluded portions are replaced with zero input) and four initial cells. Input saliency based methods like HiPe are more transparently interpretable than input optimisation, as they explicitly show which areas of the input image were more or less important in determining the output for each class. We use HiPe in preference to other input saliency based explanatory techniques as it is much quicker than similar perturbation-based saliency methods for multiple large images containing relatively small salient features, as is the case with WSIs, and is more precise than gradient-based methods which

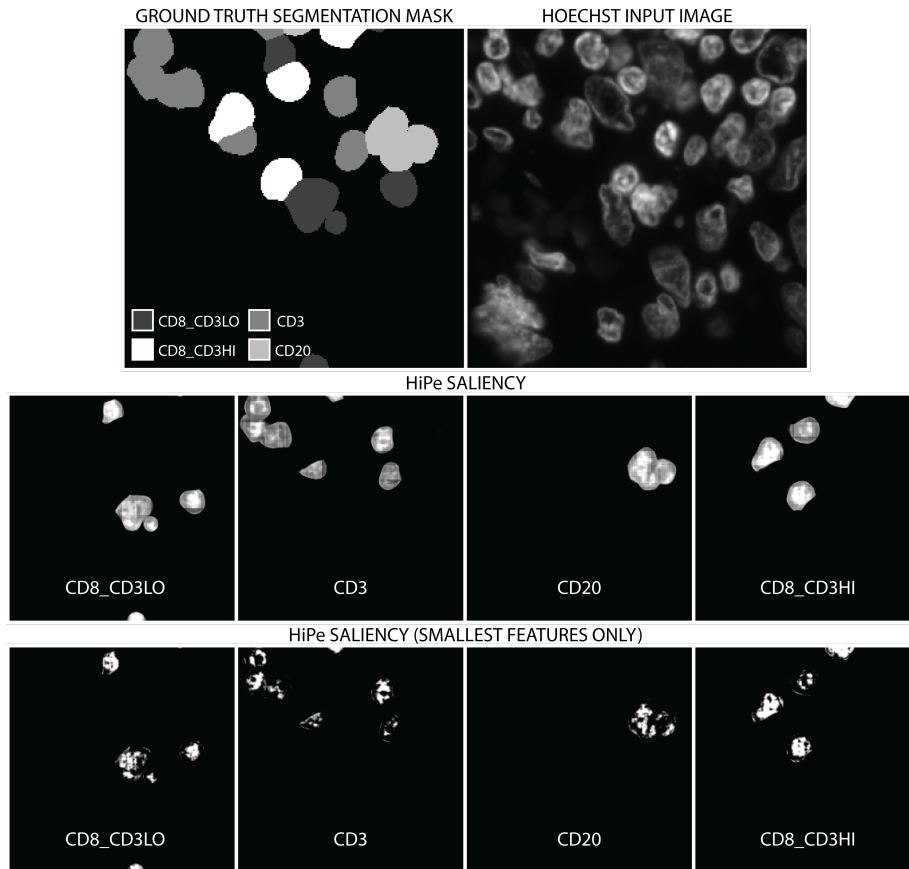


Figure 4: Labeled immune cell mask from multiplex immunofluorescence image (top left) and corresponding Hoechst 33342 stained patch (top right). Below, HiPe [8] saliency maps for each.

are often indistinct.

We found that larger salient regions were comprised of the cells themselves, as would be expected – but more interestingly, that the most salient regions were smaller, appearing to cluster in the nuclei of the salient cells. This supports our conclusion that the model is using morphological features of the chromatin made visible by Hoechst 33342 staining to perform the classification. We also note that the model does not find regions outwith the cells in question salient, showing that the proximity or morphology of nearby cells or tissue structures is not used to inform the segmentation at all.

In this work we show that with new explicability techniques, neural networks can be valuable tools for discovery as well as for automation. We demonstrate for the first time that it is possible to identify different lymphocyte protein expressions from morphological features only and present a deep learning methodology

to achieve this, which we hope will have significant impact in digital pathology.

We intend to apply proven prognostic metrics such as immune cell infiltration evaluation to slides labelled using our method, with the goal of drastically reducing the cost of immune profiling and thereby allowing more patients to benefit. Future work will include exploring semi-supervised and unsupervised approaches to classification via clustering to reduce labelling burden when training new models, alongside extending and applying our approach to other cancers and proteins.

5.2 Code Availability

All code is available at github.com/jessicamarycooper/ICAIRD.

5.3 Data Availability

The data that support the findings of this study are available from the corresponding author upon reasonable request.

6 Acknowledgements

This work is supported by the Industrial Centre for AI Research in digital Diagnostics (iCAIRD) which is funded by Innovate UK on behalf of UK Research and Innovation (UKRI) [project number: 104690] and NHS Lothian.

7 Author Contributions

All authors contributed to conceptualisation, analysis, reviewing and editing. OA and DH were responsible for funding acquisition and resources, administration and supervision. Data curation, imaging methodology and investigation were done by JC and IU. IU wrote the Multiplexed Immunofluorescence (mIF) Protocol. JC wrote the software and the remainder of the paper. Deep learning methodology and visualisation was done by JC.

8 Competing Interests

The authors declare that there are no competing interests.

References

- [1] Md Zahangir Alom, Mahmudul Hasan, Chris Yakopcic, Tarek M Taha, and Vijayan K Asari. Recurrent residual convolutional neural network based on U-Net (R2U-Net) for medical image segmentation. February 2018.

- [2] Mihaela Angelova, Bernhard Mlecnik, Angela Vasaturo, Gabriela Bindea, Tessa Fredriksen, Lucie Lafontaine, Bénédicte Buttard, Erwan Morgand, Daniela Bruni, Anne Jouret-Mourin, Catherine Hubert, Alex Kartheuser, Yves Humblet, Michele Ceccarelli, Najeeb Syed, Francesco M Marincola, Davide Bedognetti, Marc Van den Eynde, and Jérôme Galon. Evolution of metastases in space and time under immune selection. *Cell*, 175(3):751–765.e16, October 2018.
- [3] Peter Bankhead, Maurice B Loughrey, José A Fernández, Yvonne Dombrowski, Darragh G McArt, Philip D Dunne, Stephen McQuaid, Ronan T Gray, Liam J Murray, Helen G Coleman, Jacqueline A James, Manuel Salto-Tellez, and Peter W Hamilton. QuPath: Open source software for digital pathology image analysis. *Sci. Rep.*, 7(1):16878, December 2017.
- [4] Daniela Bruni, Helen K Angell, and Jérôme Galon. The immune contexture and immunoscore in cancer prognosis and therapeutic efficacy. *Nat. Rev. Cancer*, 20(11):662–680, November 2020.
- [5] Kenny H Cha, Lubomir M Hadjiiski, Ravi K Samala, Heang-Ping Chan, Richard H Cohan, Elaine M Caoili, Chintana Paramagul, Ajjai Alva, and Alon Z Weizer. Bladder cancer segmentation in CT for treatment response assessment: Application of Deep-Learning convolution neural Network-A pilot study. *Tomography*, 2(4):421–429, December 2016.
- [6] Brad Chazotte. Labeling nuclear DNA using DAPI. *Cold Spring Harb. Protoc.*, 2011(1):db.prot5556, January 2011.
- [7] Brad Chazotte. Labeling nuclear DNA with hoechst 33342. *Cold Spring Harb. Protoc.*, 2011(1):db.prot5557, January 2011.
- [8] Jessica Cooper, Ognjen Arandjelović, and David Harrison. Believe the HiPe: Hierarchical perturbation for fast and robust explanation of black box models. February 2021.
- [9] Jérôme Galon and Anastasia Lanzi. Immunoscore and its introduction in clinical practice. *Q. J. Nucl. Med. Mol. Imaging*, 64(2):152–161, June 2020.
- [10] Jérôme Galon, Bernhard Mlecnik, Gabriela Bindea, Helen K Angell, Anne Berger, Christine Lagorce, Alessandro Lugli, Inti Zlobec, Arndt Hartmann, Carlo Bifulco, Iris D Nagtegaal, Richard Palmqvist, Giuseppe V Masucci, Gerardo Botti, Fabiana Tatangelo, Paolo Delrio, Michele Maio, Luigi Laghi, Fabio Grizzi, Martin Asslaber, Corrado D’Arrigo, Fernando Vidal-Vanaclocha, Eva Zavadova, Lotfi Chouchane, Pamela S Ohashi, Sara Hafezi-Bakhtiari, Bradley G Wouters, Michael Roehrl, Linh Nguyen, Yutaka Kawakami, Shoichi Hazama, Kiyotaka Okuno, Shuji Ogino, Peter Gibbs, Paul Waring, Noriyuki Sato, Toshihiko Torigoe, Kyogo Itoh, Prabhu S Patel, Shilin N Shukla, Yili Wang, Scott Kopetz, Frank A Sinicrope, Viorel Scripcariu, Paolo A Ascierto, Francesco M Marincola, Bernard A Fox, and

- Franck Pagès. Towards the introduction of the 'immunoscore' in the classification of malignant tumours. *J. Pathol.*, 232(2):199–209, January 2014.
- [11] Kaiming He, Xiangyu Zhang, Shaoqing Ren, and Jian Sun. Deep residual learning for image recognition. *arXiv [cs.CV]*, December 2015.
- [12] Ryoichi Koga, Noriaki Hashimoto, Tatsuya Yokota, Masato Nakaguro, Kei Kohno, Shigeo Nakamura, Ichiro Takeuchi, and Hidekata Hontani. Detection of DLBCL regions in H&E stained whole slide pathology images using bayesian U-Net. In *International Forum on Medical Imaging in Asia 2021*, volume 11792, page 1179203. International Society for Optics and Photonics, April 2021.
- [13] Yan Kong, Georgi Z Genchev, Xiaolei Wang, Hongyu Zhao, and Hui Lu. Nuclear segmentation in histopathological images using Two-Stage stacked U-Nets with attention mechanism. *Front Bioeng Biotechnol*, 8:573866, October 2020.
- [14] Shyam Lal, Devikalyan Das, Kumar Alabhya, Anirudh Kanfode, Aman Kumar, and Jyoti Kini. NucleiSegNet: Robust deep learning architecture for the nuclei segmentation of liver cancer histopathology images. *Comput. Biol. Med.*, 128:104075, January 2021.
- [15] Zhang Li, Jiehua Zhang, Tao Tan, Xichao Teng, Xiaoliang Sun, Yang Li, Lihong Liu, Yang Xiao, Byungjae Lee, Yilong Li, Qianni Zhang, Shujiao Sun, Yushan Zheng, Junyu Yan, Ni Li, Yiyu Hong, Junsu Ko, Hyun Jung, Yanling Liu, Yu-Cheng Chen, Ching-Wei Wang, Vladimir Yurovskiy, Pavel Maevskikh, Vahid Khanagha, Yi Jiang, Xiangjun Feng, Zhihong Liu, Daiqiang Li, Peter J Schüffler, Qifeng Yu, Hui Chen, Yuling Tang, and Geert Litjens. Deep learning methods for lung cancer segmentation in whole-slide histopathology images – the ACDC@LungHP challenge 2019. August 2020.
- [16] Tsung-Yi Lin, Priya Goyal, Ross Girshick, Kaiming He, and Piotr Dollar. Focal loss for dense object detection. *IEEE Trans. Pattern Anal. Mach. Intell.*, 42(2):318–327, February 2020.
- [17] Ilya Loshchilov and Frank Hutter. Decoupled weight decay regularization. November 2017.
- [18] A Mahbod, G Schaefer, I Ellinger, R Ecker, Örjan Smedby, and Chunliang Wang. A Two-Stage U-Net algorithm for segmentation of nuclei in H&E-Stained tissues. In *15th European Congress on Digital Pathology, ECDP 2019, Warwick, United Kingdom 10-13 April 2019*, pages 75–82. Springer Verlag, 2019.
- [19] Bernhard Mlecnik, Marc Van den Eynde, Gabriela Bindea, Sarah E Church, Angela Vasaturo, Tessa Fredriksen, Lucie Lafontaine, Nacilla Haicheur,

- Florence Marliot, Daphné Debetancourt, Géraldine Pairet, Anne Jouret-Mourin, Jean-Francois Gigot, Catherine Hubert, Etienne Danse, Cristina Dragean, Javier Carrasco, Yves Humblet, Vii Valge-Archer, Anne Berger, Franck Pagès, Jean-Pascal Machiels, and Jérôme Galon. Comprehensive intrametastatic immune quantification and major impact of immunoscore on survival. *J. Natl. Cancer Inst.*, 110(1), January 2018.
- [20] Stanislav Nikolov, Sam Blackwell, Alexei Zverovitch, Ruheena Mendes, Michelle Livne, Jeffrey De Fauw, Yojan Patel, Clemens Meyer, Harry Askham, Bernardino Romera-Paredes, Christopher Kelly, Alan Karthikesalingam, Carlton Chu, Dawn Carnell, Cheng Boon, Derek D’Souza, Syed Ali Moinuddin, Bethany Garie, Yasmin McQuinlan, Sarah Ireland, Kiarna Hampton, Krystle Fuller, Hugh Montgomery, Geraint Rees, Mustafa Suleyman, Trevor Back, Cían Hughes, Joseph R Ledsam, and Olaf Ronneberger. Deep learning to achieve clinically applicable segmentation of head and neck anatomy for radiotherapy. September 2018.
- [21] Kay R J Oskal, Martin Risdal, Emilius A M Janssen, Erling S Undersrud, and Thor O Gulsrud. A u-net based approach to epidermal tissue segmentation in whole slide histopathological images. *SN Applied Sciences*, 1(7):672, June 2019.
- [22] F Otto and K C Tsou. A comparative study of DAPI, DIPI, and hoechst 33258 and 33342 as chromosomal DNA stains. *Stain Technol.*, 60(1):7–11, January 1985.
- [23] Edwin R Parra, Naohiro Uraoka, Mei Jiang, Pamela Cook, Don Gibbons, Marie-Andrée Forget, Chantale Bernatchez, Cara Haymaker, Ignacio I Wistuba, and Jaime Rodriguez-Canales. Validation of multiplex immunofluorescence panels using multispectral microscopy for immune-profiling of formalin-fixed and paraffin-embedded human tumor tissues. *Sci. Rep.*, 7(1):13380, October 2017.
- [24] Stephen S Raab. The Cost-Effectiveness of immunohistochemistry. *Arch. Pathol. Lab. Med.*, 124(8):1185–1191, August 2000.
- [25] Anthony E Rizzardi, Arthur T Johnson, Rachel Isaksson Vogel, Stefan E Pambuccian, Jonathan Henriksen, Amy Pn Skubitz, Gregory J Metzger, and Stephen C Schmechel. Quantitative comparison of immunohistochemical staining measured by digital image analysis versus pathologist visual scoring. *Diagn. Pathol.*, 7:42, June 2012.
- [26] Olaf Ronneberger, Philipp Fischer, and Thomas Brox. U-Net: Convolutional networks for biomedical image segmentation. May 2015.
- [27] Uwe Schmidt, Martin Weigert, Coleman Broaddus, and Gene Myers. Cell detection with star-convex polygons. June 2018.

- [28] Karen Simonyan, Andrea Vedaldi, and Andrew Zisserman. Deep inside convolutional networks: Visualising image classification models and saliency maps. December 2013.
- [29] Farhana Sultana, Abu Sufian, and Paramartha Dutta. Evolution of image segmentation using deep convolutional neural network: A survey. *Knowledge-Based Systems*, 201-202:106062, August 2020.
- [30] Wei Chang Colin Tan, Sanjna Nilesh Nerurkar, Hai Yun Cai, Harry Ho Man Ng, Duoduo Wu, Yu Ting Felicia Wee, Jeffrey Chun Tatt Lim, Joe Yeong, and Tony Kiat Hon Lim. Overview of multiplex immunohistochemistry/immunofluorescence techniques in the era of cancer immunotherapy. *Cancer Commun.*, 40(4):135–153, April 2020.
- [31] Janis M Taube, Guray Akturk, Michael Angelo, Elizabeth L Engle, Sacha Gnjjatic, Shirley Greenbaum, Noah F Greenwald, Cyrus V Hedvat, Travis J Hollmann, Jonathan Juco, Edwin R Parra, Marlon C Rebelatto, David L Rimm, Jaime Rodriguez-Canales, Kurt A Schalper, Edward C Stack, Cláudia S Ferreira, Konstanty Korski, Ana Lako, Scott J Rodig, Emanuel Schenck, Keith E Steele, Michael J Surace, Michael T Tetzlaff, Katharina von Loga, Ignacio I Wistuba, Carlo B Bifulco, and Society for Immunotherapy of Cancer (SITC) Pathology Task Force. The society for immunotherapy of cancer statement on best practices for multiplex immunohistochemistry (IHC) and immunofluorescence (IF) staining and validation. *J Immunother Cancer*, 8(1), May 2020.
- [32] Stefano Trebeschi, Joost J M van Griethuysen, Doenja M J Lambregts, Max J Lahaye, Chintan Parmar, Frans C H Bakers, Nicky H G M Peters, Regina G H Beets-Tan, and Hugo J W L Aerts. Deep learning for Fully-Automated localization and segmentation of rectal cancer on multiparametric MR. *Sci. Rep.*, 7(1):5301, July 2017.
- [33] Marc Van den Eynde, Bernhard Mlecnik, Gabriela Bindea, Tessa Fredriksen, Sarah E Church, Lucie Lafontaine, Nacilla Haicheur, Florence Marliot, Mihaela Angelova, Angela Vasaturo, Daniela Bruni, Anne Jouret-Mourin, Pamela Baldin, Nicolas Huyghe, Karin Haustermans, Annelies Debucquoy, Eric Van Cutsem, Jean-Francois Gigot, Catherine Hubert, Alex Kartheuser, Christophe Remue, Daniel Léonard, Viia Valge-Archer, Franck Pagès, Jean-Pascal Machiels, and Jérôme Galon. The link between the multiverse of immune microenvironments in metastases and the survival of colorectal cancer patients. *Cancer Cell*, 34(6):1012–1026.e3, December 2018.
- [34] Pavel Yakubovskiy. Segmentation models pytorch. https://github.com/qubvel/segmentation_models.pytorch.